Unveiling and veiling an entangled light-matter quantum state from the vacuum

Roberto Stassi,[1,2,*] Mauro Cirio,[3] Ken Funo,[2] Jorge Puebla,[4] Neill Lambert,[2] and Franco Nori[2,5,6]

[1]*Dipartimento di Scienze Matematiche e Informatiche, Scienze Fisiche e Scienze della Terra, Università di Messina, I-98166 Messina, Italy*

[2]*Theoretical Quantum Physics Laboratory, RIKEN, Wakoshi, Saitama 351-0198, Japan*

[3]*Graduate School of China Academy of Engineering Physics, Haidian District, Beijing 100193, China*

[4]*CEMS, RIKEN, Saitama 351-0198, Japan*

[5]*Center for Quantum Computing, RIKEN, Wakoshi, Saitama 351-0198, Japan*

[6]*Physics Department, The University of Michigan, Ann Arbor, Michigan 48109-1040, USA*

(Received 26 November 2021; revised 11 October 2022; accepted 27 September 2023; published 27 October 2023)

The ground state of an atom interacting with the electromagnetic field in the ultrastrong coupling regime is composed of virtual photons entangled with the atom. We propose a method to promote to real the *entire* photonic state, while preserving the entanglement with the atom. The process can be reversed, and the entangled state can be restored in the vacuum. We consider a four-level atom, with two of these levels ultrastrongly coupled to a cavity mode. The process is obtained by making use of either an ideal ultrafast pulse or a more realistic multitone π pulse that drives only the atom. An experimental realization of this proposal will not only enable the investigation of the exotic phenomena of emission of particles from the vacuum, but will also prove that *quantum superposition states* can be extracted from the vacuum. Moreover, it will allow one to inspect the ground state in the ultrastrong coupling regime, and to generate on-demand entangled states for quantum information processing.

DOI: 10.1103/PhysRevResearch.5.043095

I. INTRODUCTION

One of the most fascinating features of quantum mechanics is that the quantum vacuum is filled with virtual particles [1]. In the presence of intense fields, the quantum vacuum can become a pure entangled state. For example, at the horizon of a black hole, where the gravitational field is very intense, the quantum vacuum is predicted to be a two-mode squeezed entangled state. Outside the event horizon, the virtual particles forming this entangled vacuum state are promoted to real at the expense of the gravitational field [2].

Using superconducting circuits [1,3–12], it is possible to generate extreme physical conditions that enable the manipulation of the quantum vacuum in a laboratory setting. In particular, it was shown [13–17] that the interaction energy of a superconducting flux qubit coupled to a cavity field can be larger than the cavity or qubit bare energies. Deep in this ultrastrong coupling regime, the ground state is a cat light-matter entangled state [18–31]. This state is not "visible" (measurable), because it is made of "virtual excitations." However, these virtual excitations generate a pressure to the external environment [32–34] which could, in principle, be probed. The quantum information of this quantum vacuum state is not accessible directly and it is not useful for quantum information tasks.

Here we propose a protocol in which the *entire* entangled cat state forming the ground state in the ultrastrong coupling regime is converted from "virtual" to "real." This is done by swapping the entanglement with the cavity field from the atomic states that ultrastrongly interacts with the cavity to other ones that do not. The swap is implemented by driving the atom with an ideal ultrafast monotone pulse or with a multitone π pulse [35–39]. Note that we never drive the cavity. After the pulse, the cat state remains in a noninteracting sector of the Hilbert space, thereby the quantum information of this quantum state now is accessible and can be directly measured. Using an identical pulse the process can be inverted, and the entangled cat state can be restored in the system ground state, becoming again nonmeasurable.

II. MODEL

Our system consists of a four-level atom, $\{|g\rangle, |e\rangle, |g'\rangle, |e'\rangle\}$, and a cavity mode with frequency ω_c. We call A the subsystem $\{|g\rangle, |e\rangle\}$, that is ultrastrongly coupled to the cavity field B, and C is the subsystem $\{|g'\rangle, |e'\rangle\}$ which does not interact [see Fig. 1(a)]. The general procedure, valid for both the ultrafast and the multitone pulse, is as follows [see Fig. 1(b)]: At t_0, we prepare the system in its ground state. Now, because of the large energy coupling, the atomic subspace A is maximally entangled with the cavity field B, forming an entangled light-matter cat state. Because the system is in its dressed ground state, it is not possible to make a measurement in order to acquire information about

*rstassi@unime.it

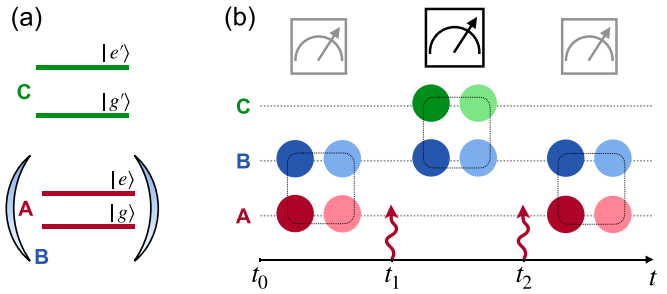

FIG. 1. (a) The system consists of a two-level system A and a cavity field B interacting deep in the ultrastrong light-matter coupling regime. The subsystem C represents the noninteracting atomic states. (b) The colored disks represent the entanglement between the subsystem A-B, and B-C at different moments. At t_0 the subsystem A is entangled with B, but this entanglement is not directly accessible. After a pulse at t_1, the cavity field B is entangled with C, and now this entanglement can be measured. After a pulse at t_2, the cavity field B is entangled again with A.

this entangled state. At t_1, a proper π pulse, sent to the atom, swaps the atomic states from the ones that interact, A, to the ones that do not interact, and that forms the subsystem C. With this process we have a swap of the entanglement from the subsystem A to the subsystem C. The entire cat state, that previously was not accessible, can now be measured. At t_2, a second pulse, equal to the first, restores the cat state to the ground state.

The Hamiltonian describing the total system is $\hat{H} = \hat{H}_{\rm R} + \hat{H}' + \hat{D}$, where the Rabi Hamiltonian

$$\hat{H}_{\rm R} = \omega_{\rm q}|e\rangle\langle e| + \omega_{\rm c}\,\hat{a}^\dagger\hat{a} + \lambda\,\hat{\sigma}_x(\hat{a} + \hat{a}^\dagger), \tag{1}$$

and $\hat{H}' = \omega_{e'g'}\,|e'\rangle\langle e'|$ describe the dynamics of the interacting and noninteracting states, respectively ($\hbar = 1$). The energy difference between the latter states is defined by $\hat{D} = \omega_{g'}(|e'\rangle\langle e'| + |g'\rangle\langle g'|)$, $\hat{\sigma}_x = |e\rangle\langle g| + |g\rangle\langle e|$ is a Pauli operator, $\hat{a}$ is the annihilation operator for the cavity mode, and $\omega_{mn} = \omega_m - \omega_n$. We set $\omega_{\rm c} = \omega_{\rm q}$ and $\lambda = 1.34\,\omega_{\rm q}$. Figure 2(b) shows the eigenstates of the total Hamiltonian $\hat{H}$. For $\lambda \gg 0.5\,\omega_{\rm c}$, the atomic states $\{|g\rangle, |e\rangle\}$ hybridize with the photonic states, and the ground state becomes an entangled cat state, $|\mathcal{C}_-\rangle \approx 1/\sqrt{2}(|+\rangle|-\alpha\rangle - |-\rangle|+\alpha\rangle)$ (red solid line). Here, $|\pm\rangle = 1/\sqrt{2}(|e\rangle \pm |g\rangle)$ are the eigenstates of $\hat{\sigma}_x$, and $|\pm\alpha\rangle = D(\pm\alpha)|0\rangle$ are photonic coherent states of light with positive and negative displacement α [40]. The colored lines in Fig. 2(b) are Fock states associated with the noninteracting subspace for when the atomic system is in the states $|g'\rangle$ and $|e'\rangle$. For clarity, other dressed eigenstates of the total Hamiltonian are not shown in Fig. 2(b).

III. ENTANGLEMENT SWAPPING

A. Swapping using an ultrafast pulse

We now present the swapping procedure in which the entanglement in the dressed light-matter ground state is mapped into entanglement in the noninteracting sector, i.e., for large

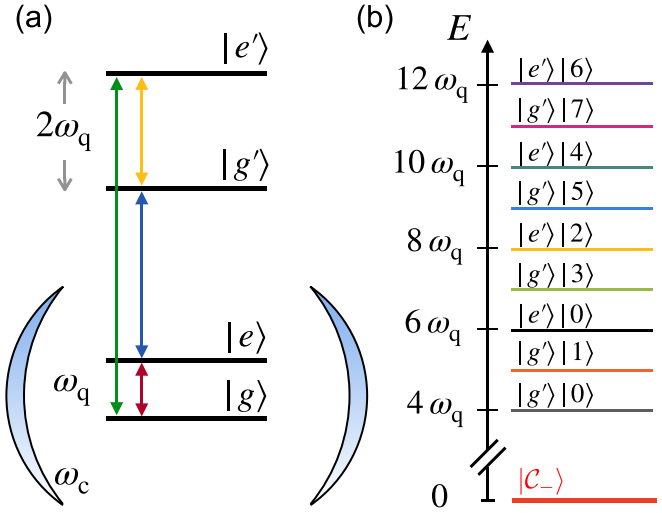

FIG. 2. (a) Four-level atomic system: states $|g\rangle$ and $|e\rangle$ interact ultrastrongly with a cavity mode. (b) Noninteracting states (colored lines) and dressed ground state $|\mathcal{C}_-\rangle$ (red line) of the total Hamiltonian $\hat{H}$. The parameters are chosen so that the atomic states $|g'\rangle$ and even number of photons are degenerate with the atomic states $|e'\rangle$ and odd number of photons.

coupling $\lambda/\omega_{\rm q} > 1$,

$$|\mathcal{C}_-\rangle \approx \frac{1}{\sqrt{2}}(\,|+\rangle\,|-\alpha\rangle - |-\rangle|+\alpha\rangle), \tag{2}$$

$$\Downarrow \qquad\qquad \Downarrow$$

$$|\mathcal{C}'_-\rangle \approx \frac{1}{\sqrt{2}}(\,|+'\rangle\,|-\alpha\rangle - |-'\rangle|+\alpha\rangle), \tag{3}$$

where $|\pm'\rangle = 1/\sqrt{2}(|g'\rangle \pm |e'\rangle)$. The swap is realized by inducing atomic transitions $\{|g\rangle, |e\rangle\} \to \{|e'\rangle, |g'\rangle\}$, using an ultrafast ideal pulse sent to the atom [Fig. 3(a)]. For the experimental realization, we show that also a multitone π pulse can efficiently lead to the same result [Fig. 3(b)]. Figure 3 displays the dynamical evolution of the Fock state populations for the states $|g', n\rangle$ and $|e', n\rangle$ (solid lines), which can be compared with the Fock states associated with $|g, n\rangle$ and $|e, n\rangle$ (dotted lines) representing the bare populations of the state $|\mathcal{C}_-\rangle$.

The ultrafast pulse is given by

$$\hat{H}_{\rm p} = \varepsilon_{\rm p}(\hat{\sigma}_{eg'} + \hat{\sigma}_{ge'} + \text{H.c.}), \tag{4}$$

with

$$\varepsilon_{\rm p} = \pi\varepsilon\,\exp\left[-(t - t_i)^2/2A_{\rm p}^2\right]/A_{\rm p}\sqrt{2\pi}, \tag{5}$$

$\hat{\sigma}_{mn} = |m\rangle\langle n|$, $\varepsilon = 1/2$, $A_{\rm p} = 6 \times 10^{-3}/\omega_{\rm q}$, and t_i (with $i = 1, 2$) is the center of the Gaussian pulse. In this simulation no dissipation is taken into account.

At $t = 0$, we prepare the system in the dressed state $|\mathcal{C}_-\rangle$. In Fig. 3(a), at $\tilde{t}_1 = 1$ (up red arrow), with $\tilde{t} = \omega_{\rm q}t/2\pi$, an ultrafast pulse depopulates state $|\mathcal{C}_-\rangle$ and populates the Fock states associated with $|g'\rangle$ and $|e'\rangle$ (solid lines). The latter states match exactly the ones associated with $|g\rangle$ and $|e\rangle$ (dotted lines) before the pulse was sent. This proves that the cat state now is an entangled state within the subspace $\{|g'\rangle, |e'\rangle\}$. The photonic contribution before and after the pulse remains almost unchanged, as shown in Eqs. (2) and (3). The cat state

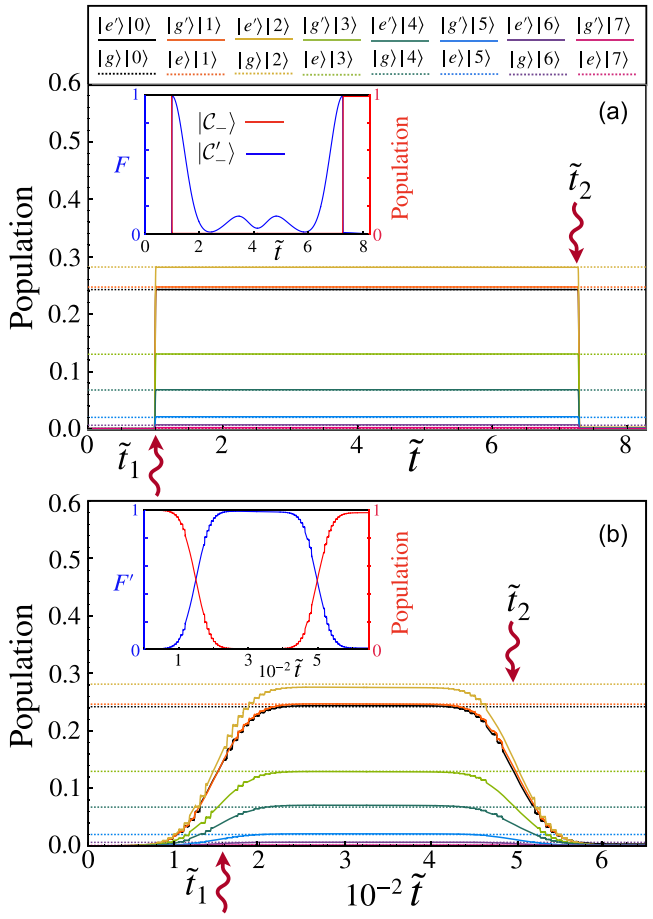

FIG. 3. Dynamics of the Fock state populations associated with the atomic states $|g'\rangle$ and $|e'\rangle$ (solid lines) when the atom is initially prepared in $|\mathcal{C}_-\rangle$ and is subject to an ultrafast pulse (a), or a multitone pulse (b). These can be compared with the Fock states associated with $|g\rangle$ and $|e\rangle$ (dotted lines) when the state of the system is $|\mathcal{C}_-\rangle$. Here, $\omega_{g'e} = 3\omega_q$, $\omega_{e'g'} = 2\omega_q$, $\lambda = 1.34\omega_q$, and $N = 7$. The inset in (a) shows the population for the $|\mathcal{C}_-\rangle$ state (red curve) and the fidelity F for the $|\mathcal{C}'_-\rangle$ state (blue curve). The inset in (b) shows the same quantities, but the fidelity F' is now calculated by eliminating the relative phases because the revival of the fidelity, which is the same as in the inset in (a), produces very rapid oscillations in a longer simulation, making these difficult to resolve.

is now visible to an external observer, because the photons are real and can be detected. After the first pulse is sent at $\tilde{t}_1$, superpositions within the state experience a phase shift [41,42] [see inset Fig. 3(a)]. At $\tilde{t}_2 = \tilde{t}_1 + \tilde{t}_d$ (down red arrow), with $\tilde{t}_d = \omega_q/|\omega_{e'g'} - \omega_c|$, the state returns in phase with the corresponding light-matter ground state $|\mathcal{C}_-\rangle$ and a second pulse equal to the first brings the cat state back to its original "virtual form" encoded in the ground state of the Rabi Hamiltonian $|\mathcal{C}_-\rangle$.

B. Swapping using a multitone pulse

Figure 3(b) shows the dynamical evolution of the system when a multitone π pulse is sent to the atom and the state of the system is initially $|\mathcal{C}_-\rangle$. Here, we consider more experimentally realistic conditions, taking into account also the transition $|g\rangle \leftrightarrow |e\rangle$ and $|g'\rangle \leftrightarrow |e'\rangle$ in the Hamiltonian of the pulse, and including environmental effects [27]. The pulse is described by

$$\hat{H}_p = \varepsilon_p \sum_{i=0}^{N} \cos[\omega_{p_i}(t - t_s)](\hat{\sigma}_{eg'} + \hat{\sigma}_{ge'} + \hat{\sigma}_{ge} + \hat{\sigma}_{g'e'} + \text{H.c.}), \tag{6}$$

where $\varepsilon = 1$, $A_p = 50/\omega_q$, $\omega_{p_i} = \omega_{\mathcal{C}_-} - \omega_i$, ω_i are the frequencies of $|g', 2i+1\rangle$ and $|e', 2i\rangle$, and $\omega_{\mathcal{C}_-}$ is the ground state energy. We note that the transitions described in the pulse Hamiltonian satisfy the optical selection rules for a flux qubit in its optimal point (see Appendix A).

At $\tilde{t}_1 = 150$ (up red arrow), the first pulse is sent to the atom, gradually populating the noninteracting sector until the full entanglement is swapped. At $\tilde{t}_2 = 500$ (down red arrow), a second pulse equal to the first restores (not perfectly because of dissipation) the original $|\mathcal{C}_-\rangle$ state. We note that, because the state $|\mathcal{C}_-\rangle$ is the system ground state, dissipation would automatically restore the initial state within the relaxation time associated with the atom. The inset in Fig. 3(b) shows the population (red curve) of the $|\mathcal{C}_-\rangle$ state and the fidelity F' between the state of the system and the state $|\mathcal{C}_{\text{ideal}}\rangle = (\hat{\sigma}_{e'g} + \hat{\sigma}_{g'e})|\mathcal{C}_-\rangle$.

IV. PERFORMANCE OF THE PROTOCOL USING THE MULTITONE PULSE

To quantify the performance of this protocol, we now calculate the amount of entanglement that can be transferred from the initial state $|\mathcal{C}_-\rangle$ to the state $|\mathcal{C}'_-\rangle$. In Figure 4(a), we show the von Neumann entropy [43] calculated after sending a multitone π pulse with seven (green dots) and nine (blue dots) frequencies, and after postselecting onto the $\{|g'\rangle, |e'\rangle\}$ subspace. This approach is valid only when the populations in the $|g\rangle$ and $|e\rangle$ states are zero after the swapping procedure. However, when there is a small residual population, it is still a good indicator of the amount of entanglement transferred from virtual to real [see inset in Fig. 4(a)].

These results can be compared with the entropy calculated for the subsystem $\{|g\rangle, |e\rangle\}$, when the state of the system is $|\mathcal{C}_-\rangle$ (red dots). Note that for couplings in the range $0.5 < \lambda/\omega_q < 0.8$, going from seven to nine pulses does not lead to improvements. However, for $\lambda/\omega_q > 0.8$, the number of photons in the ground state increases, and using nine frequencies in the pulse outperforms the seven-frequencies case.

Figure 4(b) displays the fidelity for the state of the system calculated with respect to a target entangled state with $\alpha = \lambda/\omega_c$ [27], after sending the multitone π pulse with seven (green dots) and nine (blue dots) frequencies. This result can be compared with the fidelity for the state $|\mathcal{C}_-\rangle$ (red dots). As before, for large coupling, increasing the number of frequencies in the pulse corresponds to an increase in fidelity.

Our proposal can be realized using a flux qubit coupled to a waveguide or *LC* resonator (see Appendix A). When the reduced external flux that threads the flux qubit is $f = 0.5$ [44,45], the allowed transitions become $|g\rangle \leftrightarrow |e\rangle$, $|g\rangle \leftrightarrow |e'\rangle$,

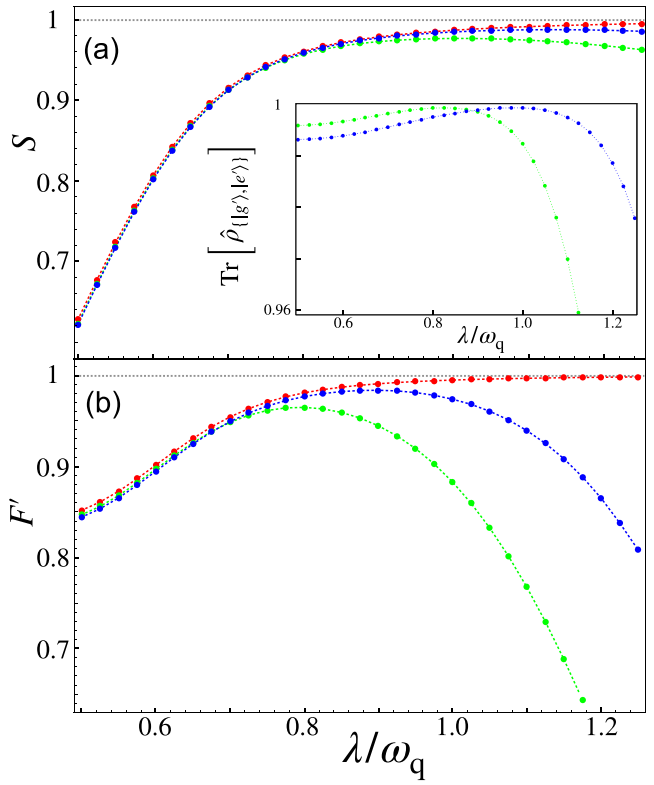

FIG. 4. (a) Entanglement entropy S between the field and the atomic subspace $\{|g'\rangle, |e'\rangle\}$ after a multitone π pulse with seven frequencies (green dots) and nine frequencies (blue dots) is sent to the atom. The atom is initially prepared in the $|\mathcal{C}_-\rangle$ state. It is possible to compare this to the entropy relative to the subspace $\{|g\rangle, |e\rangle\}$, when the state of the system is $|\mathcal{C}_-\rangle$ (red dots). The inset shows the trace of the density matrix $\hat{\rho}_{\{|g'\rangle,|e'\rangle\}}$ for the subspace $\{|g'\rangle, |e'\rangle\}$, after a multitone π pulse with seven (green dots) and nine (blue dots) frequencies is sent. (b) Fidelity F' (eliminating relative phases) between an ideal cat state entangled with the atom and the system state after a π pulse with seven (green dots) and nine frequencies (blue dots) is sent to the atom. The ideal cat state is generated choosing $\alpha = \lambda/\omega_c$. In (a) and (b) we consider the interacting states $\{|g\rangle, |e\rangle\}$ at higher energy with respect to $\{|g'\rangle, |e'\rangle\}$. Here $\omega_g = 9\,\omega_q$, $\omega_c = \omega_q/2$, and $\omega_{e'g'} = \omega_q$.

$|e\rangle \leftrightarrow |g'\rangle$, and $|g'\rangle \leftrightarrow |e'\rangle$. These optical selection rules are the ones that we consider when we define the multitone pulse.

V. CONCLUSIONS

In this work, we proposed a protocol to unveil the virtual entangled ground state of a two-level system ultrastrongly coupled to a cavity mode. To unveil and make the state visible and measurable, the entangled partner is swapped using an ultrafast pulse or a multitone π pulse. With this proposal, not only is it possible to explore the ground state of the Rabi Hamiltonian in the ultrastrong coupling regime, but it can also lead to an efficient way to generate photonic cat states on demand, which can be an important resource for quantum computation and other quantum technologies [46,47]. In the case of a black-hole horizon, after the promotion from virtual to real of particles, the quantum information of the vacuum state is apparently lost, giving rise to the quantum information paradox [48]. Understanding and solving this paradox is crucial to have a theory of quantum mechanics consistent with Einstein general relativity. Our proposal could potentially enable experiments using superconducting qubits which mimic the vacuum state in the proximity of a black hole and the particle emission from its horizon, giving the chance to investigate, in laboratory conditions, the black-hole information paradox [49–51].

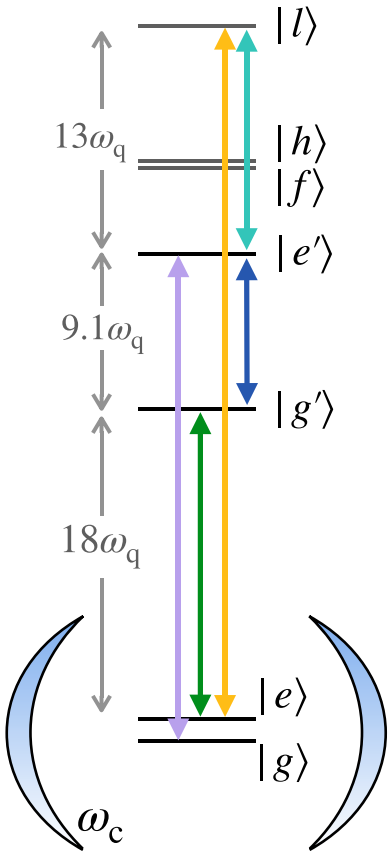

FIG. 5. (a) Energy diagram of a flux qubit characterized by the parameters $E_C = 2.8$ GHz, $E_J = 40E_C$, $\alpha = 0.8$, and $f = 0.5$.

ACKNOWLEDGMENTS

F.N. is supported in part by Nippon Telegraph and Telephone Corporation (NTT) Research, the Japan Science and Technology Agency (JST) [via the Quantum Leap Flagship Program (Q-LEAP), and the Moonshot R&D Grant No. JPMJMS2061], the Asian Office of Aerospace Research and Development (AOARD) (via Grant No. FA2386-20-1-4069), and the Foundational Questions Institute Fund (FQXi) via Grant No. FQXi-IAF19-06. M.C. acknowledges support from NSFC (Grant No. 11935012). R.S. acknowledges the Army Research Office (ARO) (Grant No. W911NF1910065).

APPENDIX A: FLUX QUBIT CONFIGURATION

The protocol analyzed in the main text can be realized using a flux qubit coupled to either a waveguide or to an *LC* resonator. An *LC* resonator is preferred because it operates in a single mode, preventing unwanted transitions to higher modes. Figure 5(a) represents the lowest seven

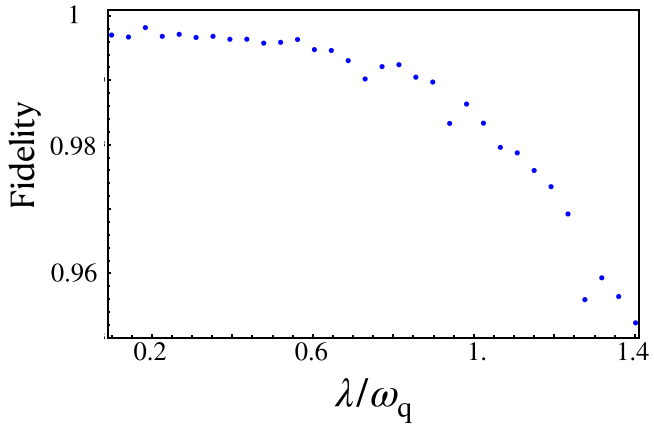

FIG. 6. Fidelity as a function of the normalized light-matter coupling λ/ω_q, between the dressed ground state and the state generated after sending the multimode pulse with eight frequencies. Here we used $\omega_{eg} = \omega_q = 1$, $\omega_{g'e} = 18\,\omega_q$, $\omega_{e'g'} = 9.1\,\omega_q$, $\omega_{le'} = 13\,\omega_q$, $M_{eg} = 0.83$, $M_{e'g'} = 0.5$, $M_{e'g} = 0.137$, $M_{g'e} = 0.116$, $M_{le} = 0.22$, and $M_{le'} = 0.3$. For this simulation we adopted a Hilbert space with eight photons.

eigenstates of a flux qubit with charging energy $E_C = 2.8$ GHz, Josephson energy $E_J = 40E_C$, flux qubit charge ratio $\alpha = 0.8$, and a reduced external flux $f = 0.5$. With these parameters, the transition $|g\rangle \leftrightarrow |e\rangle$ has frequency $\omega_q \approx 1$ GHz, $\omega_{g'e} \approx 18\omega_q$, and $\omega_{e'g'} \approx 9.1\omega_q$. Optical selection rules allow the transitions $|g\rangle \leftrightarrow |e\rangle$, $|g\rangle \leftrightarrow |e'\rangle$, $|e\rangle \leftrightarrow |g'\rangle$, and $|g'\rangle \leftrightarrow |e'\rangle$. The transitions are determined by the matrix elements $M_{ij} = \langle i|\sin(2\pi f + 2\varphi_-)|j\rangle$, where φ_- is the difference between the fluxes crossing the Josephson junctions. The calculated matrix elements have values $M_{eg} = 0.83$, $M_{e'g'} = 0.5$, $M_{g'e} = 0.14$, and $M_{e'g} = 0.12$. The transitions $|e\rangle \leftrightarrow |l\rangle$ and $|e'\rangle \leftrightarrow |l\rangle$ are also allowed with transition energy $\omega_{le'} \approx 13\,\omega_q$, and matrix transition elements $M_{el} = 0.22$ and $M_{e'l} = 0.3$.

If the cavity frequency is tuned to the frequency transition $|g\rangle \leftrightarrow |e\rangle$, this transition can achieve the ultrastrong coupling regime. The states $|g'\rangle$ and $|e'\rangle$ can represent the atomic noninteracting sector for two reasons: (i) their allowed atomic transitions are much detuned with respect to the cavity; and (ii) the corresponding matrix elements M_{ij} are smaller than M_{eg}.

Using this configuration for a flux qubit, in Fig. 6 is shown the numerically calculated fidelity between the dressed Rabi ground state and the state generated using a multimode pulse for different couplings. The procedure is the same as in the main text. Notice that in these numerical results we take into account all the possible interactions among the states $|g\rangle$, $|e\rangle$, $|g'\rangle$, $|e'\rangle$, and $|l\rangle$. Here the system Hamiltonian is

$$\hat{H} = \sum_{i,j=g,e,g',e',l} \omega_{ig}|i\rangle\langle i| + \lambda_{ij}\,|i\rangle\langle j|(\hat{a} + \hat{a}^\dagger) \tag{A1}$$

with coupling $\lambda_{ij} = \lambda M_{ij}/M_{eg}$, such that $\lambda_{eg} = \lambda$. Frequencies and transition matrix elements correspond to the one calculated above for a flux qubit. Using these parameters, the Hilbert space becomes too large to numerically compute the system dynamics. For this reason we reduced the dimension of the photonic subspace, now taking into account eight photons (instead of the 25 considered in the main text).

The drive Hamiltonian is

$$\hat{H}_p = \varepsilon_p \sum_{i=0}^{N} \cos[\omega_{p_i}(t - t_s)](\hat{\sigma}_{eg'} + \hat{\sigma}_{ge'} + \hat{\sigma}_{ge} \tag{A2}$$

$$+ \hat{\sigma}_{g'e'} + \hat{\sigma}_{el} + \hat{\sigma}_{e'l} + \text{H.c.}), \tag{A3}$$

with $\hat{\sigma}_{mn} = |m\rangle\langle n|$, $\varepsilon_p = \pi\varepsilon\,\exp[-(t - t_i)^2/2A_p^2]/A_p\sqrt{2\pi}$, where $\varepsilon = 1$, $A_p = 50/\omega_q$, $\omega_{p_i} = \omega_{\mathcal{C}_-} - \omega_i$, ω_i are the frequencies of $|g', 2i+1\rangle$ and $|e', 2\,i\rangle$, $\omega_{\mathcal{C}_-}$ is the ground state energy, and t_i is the center of the Gaussian pulse.

APPENDIX B: ENVIRONMENTAL EFFECTS

The dissipation in the numerical simulations in the main text was modeled using the master equation [27],

$$\dot{\hat{\rho}} = -i[\hat{H}_S, \hat{\rho}] + \sum_k \sum_{m,\,n>m} \Gamma_{mn}^{(k)} \mathcal{D}[|m\rangle\langle n|]\hat{\rho} \tag{B1}$$

$$+ \sum_k \gamma_\varphi^{(k)} \mathcal{D}\left[\sum_m \langle m|\hat{S}_z^{(k)}|m\rangle\,|m\rangle\langle m|\right]\hat{\rho},$$

where $\hat{H}_S = \hat{H} + \hat{H}_p$, $\mathcal{D}[\hat{O}]\hat{\rho} = (2\hat{O}\hat{\rho}\,\hat{O}^\dagger - \hat{O}^\dagger\hat{O}\hat{\rho} - \hat{\rho}\,\hat{O}^\dagger\hat{O})/2$ is the Lindblad superoperator, $|m\rangle$ are eigenstates of $\hat{H}$, and $\hat{\rho}$ is the density matrix of the system,

$$\begin{aligned} \Gamma_{mn}^{(k)} &= \gamma^{(k)}|\langle m|\hat{S}^{(k)}|n\rangle|^2, \\ \hat{S}^{(k)} &\in \{\hat{\sigma}_{eg'}, \hat{\sigma}_{ge'}, \hat{\sigma}_{eg}, \hat{\sigma}_{e'g'}, \hat{a} + \hat{a}^\dagger\}, \\ \hat{S}_z^{(k)} &\in \{\hat{\sigma}_{ee} - \hat{\sigma}_{gg}, \hat{\sigma}_{e'e'} - \hat{\sigma}_{g'g'}, \hat{a}^\dagger\hat{a}\}, \end{aligned} \tag{B2}$$

where $\gamma^{(k)}$ and $\gamma_\varphi^{(k)}$ are the relaxation and pure dephasing rates with $\gamma^{(k)} = \gamma_\varphi^{(k)} = 10^{-5}\,\omega_q$.

[1] P. D. Nation, J. R. Johansson, M. P. Blencowe, and F. Nori, "*Colloquium*: Stimulating uncertainty: Amplifying the quantum vacuum with superconducting circuits," Rev. Mod. Phys. **84**, 1 (2012).

[2] S. W. Hawking, Black hole explosions? Nature (London) **248**, 30 (1974).

[3] J. M. Martinis, M. H. Devoret, and J. Clarke, Energy-level quantization in the zero-voltage state of a current-biased Josephson junction, Phys. Rev. Lett. **55**, 1543 (1985).

[4] M. H. Devoret, J. M. Martinis, and J. Clarke, Measurements of macroscopic quantum tunneling out of the zero-voltage state of a current-biased Josephson junction, Phys. Rev. Lett. **55**, 1908 (1985).

[5] Y. Nakamura, Y. A. Pashkin, and J. Tsai, Coherent control of macroscopic quantum states in a single-Cooper-pair box, Nature (London) **398**, 786 (1999).

[6] A. Blais, R.-S. Huang, A. Wallraff, S. M. Girvin, and R. J. Schoelkopf, Cavity quantum electrodynamics for

superconducting electrical circuits: An architecture for quantum computation, Phys. Rev. A **69**, 062320 (2004).

[7] J. You and F. Nori, Atomic physics and quantum optics using superconducting circuits, Nature (London) **474**, 589 (2011).

[8] P. Krantz, M. Kjaergaard, F. Yan, T. P. Orlando, S. Gustavsson, and W. D. Oliver, A quantum engineer's guide to superconducting qubits, Appl. Phys. Rev. **6**, 021318 (2019).

[9] J. M. Martinis, M. H. Devoret, and J. Clarke, Quantum Josephson junction circuits and the dawn of artificial atoms, Nat. Phys. **16**, 234 (2020).

[10] M. Kjaergaard, M. E. Schwartz, J. Braumüller, P. Krantz, J. I.-J. Wang, S. Gustavsson, and W. D. Oliver, Superconducting qubits: Current state of play, Annu. Rev. Condens. Matter Phys. **11**, 369 (2020).

[11] R. Stassi, M. Cirio, and F. Nori, Scalable quantum computer with superconducting circuits in the ultrastrong coupling regime, npj Quantum Inf. **6**, 67 (2020).

[12] S. Kwon, A. Tomonaga, G. Lakshmi Bhai, S. J. Devitt, and J.-S. Tsai, Gate-based superconducting quantum computing, J. Appl. Phys. **129**, 041102 (2021).

[13] T. Niemczyk, F. Deppe, H. Huebl, E. Menzel, F. Hocke, M. Schwarz, J. Garcia-Ripoll, D. Zueco, T. Hümmer, and E. Solano, Circuit quantum electrodynamics in the ultrastrong-coupling regime, Nat. Phys. **6**, 772 (2010).

[14] F. Yoshihara, T. Fuse, S. Ashhab, K. Kakuyanagi, S. Saito, and K. Semba, Superconducting qubit–oscillator circuit beyond the ultrastrong-coupling regime, Nat. Phys. **13**, 44 (2017).

[15] P. Forn-Díaz, J. J. García-Ripoll, B. Peropadre, J.-L. Orgiazzi, M. Yurtalan, R. Belyansky, C. M. Wilson, and A. Lupascu, Ultrastrong coupling of a single artificial atom to an electromagnetic continuum in the nonperturbative regime, Nat. Phys. **13**, 39 (2017).

[16] A. F. Kockum, A. Miranowicz, S. De Liberato, S. Savasta, and F. Nori, Ultrastrong coupling between light and matter, Nat. Rev. Phys. **1**, 19 (2019).

[17] P. Forn-Díaz, L. Lamata, E. Rico, J. Kono, and E. Solano, "Ultrastrong coupling regimes of light-matter interaction," Rev. Mod. Phys. **91**, 025005 (2019).

[18] M. O. Scully and M. S. Zubairy, *Quantum Optics* (Cambridge University Press, Cambridge, UK, 1999).

[19] T. C. Ralph, A. Gilchrist, G. J. Milburn, W. J. Munro, and S. Glancy, Quantum computation with optical coherent states, Phys. Rev. A **68**, 042319 (2003).

[20] A. Gilchrist, K. Nemoto, W. J. Munro, T. C. Ralph, S. Glancy, S. L. Braunstein, and G. J. Milburn, Schrödinger cats and their power for quantum information processing, J. Opt. B **6**, S828 (2004).

[21] Y.-X. Liu, L. F. Wei, and F. Nori, Generation of nonclassical photon states using a superconducting qubit in a microcavity, Europhys. Lett. **67**, 941 (2004).

[22] S. Ashhab and F. Nori, Qubit-oscillator systems in the ultrastrong-coupling regime and their potential for preparing nonclassical states, Phys. Rev. A **81**, 042311 (2010).

[23] P. Nataf and C. Ciuti, Vacuum degeneracy of a circuit QED system in the ultrastrong coupling regime, Phys. Rev. Lett. **104**, 023601 (2010).

[24] G. S. Agarwal, *Quantum Optics* (Cambridge University Press, Cambridge, UK, 2012).

[25] D. J. Wineland, "Nobel lecture: Superposition, entanglement, and raising Schrödinger's cat," Rev. Mod. Phys. **85**, 1103 (2013).

[26] M. Mirrahimi, Cat-qubits for quantum computation, C. R. Phys. **17**, 778 (2016).

[27] R. Stassi and F. Nori, Long-lasting quantum memories: Extending the coherence time of superconducting artificial atoms in the ultrastrong-coupling regime, Phys. Rev. A **97**, 033823 (2018).

[28] H.-Y. Ku, N. Lambert, F.-J. Chan, C. Emary, Y.-N. Chen, and F. Nori, Experimental test of non-macrorealistic cat states in the cloud, npj Quantum Inf. **6**, 98 (2020).

[29] Y. H. Chen, W. Qin, X. Wang, A. Miranowicz, and F. Nori, Shortcuts to adiabaticity for the quantum Rabi model: Efficient generation of giant entangled cat states via parametric amplification, Phys. Rev. Lett. **126**, 023602 (2021).

[30] Z. Y. Zhou, C. Gneiting, J. Q. You, and F. Nori, Generating and detecting entangled cat states in dissipatively coupled degenerate optical parametric oscillators, Phys. Rev. A **104**, 013715 (2021).

[31] W. Qin, A. Miranowicz, H. Jing, and F. Nori, Generating long-lived macroscopically distinct superposition states in atomic ensembles, Phys. Rev. Lett. **127**, 093602 (2021).

[32] L. Garziano, R. Stassi, A. Ridolfo, O. Di Stefano, and S. Savasta, Vacuum-induced symmetry breaking in a superconducting quantum circuit, Phys. Rev. A **90**, 043817 (2014).

[33] J. Lolli, A. Baksic, D. Nagy, V. E. Manucharyan, and C. Ciuti, Ancillary qubit spectroscopy of vacua in cavity and circuit quantum electrodynamics, Phys. Rev. Lett. **114**, 183601 (2015).

[34] M. Cirio, K. Debnath, N. Lambert, and F. Nori, Amplified optomechanical transduction of virtual radiation pressure, Phys. Rev. Lett. **119**, 053601 (2017).

[35] R. Stassi, A. Ridolfo, O. Di Stefano, M. J. Hartmann, and S. Savasta, Spontaneous conversion from virtual to real photons in the ultrastrong-coupling regime, Phys. Rev. Lett. **110**, 243601 (2013).

[36] O. Di Stefano, R. Stassi, L. Garziano, A. Frisk Kockum, S. Savasta, and F. Nori, Feynman-diagrams approach to the quantum Rabi model for ultrastrong cavity QED: Stimulated emission and reabsorption of virtual particles dressing a physical excitation, New J. Phys. **19**, 053010 (2017).

[37] E. Sánchez-Burillo, L. Martín-Moreno, J. J. García-Ripoll, and D. Zueco, Single photons by quenching the vacuum, Phys. Rev. Lett. **123**, 013601 (2019).

[38] Y. H. Chen, W. Qin, R. Stassi, X. Wang, and F. Nori, Fast binomial-code holonomic quantum computation with ultrastrong light-matter coupling, Phys. Rev. Res. **3**, 033275 (2021).

[39] A. Mercurio, S. De Liberato, F. Nori, S. Savasta, and R. Stassi, Flying atom back-reaction and mechanically generated photons from vacuum, arXiv:2209.10419.

[40] E. K. Irish, J. Gea-Banacloche, I. Martin, and K. C. Schwab, Dynamics of a two-level system strongly coupled to a high-frequency quantum oscillator, Phys. Rev. B **72**, 195410 (2005).

[41] A. Ridolfo, R. Vilardi, O. Di Stefano, S. Portolan, and S. Savasta, All optical switch of vacuum Rabi oscillations: The ultrafast quantum eraser, Phys. Rev. Lett. **106**, 013601 (2011).

[42] O. Di Stefano, R. Stassi, A. Ridolfo, S. Patane, and S. Savasta, Interference with coupled microcavities: Optical analog of spin 2π rotations, Phys. Rev. B **84**, 085324 (2011).

[43] R. Horodecki, P. Horodecki, M. Horodecki, and K. Horodecki, "Quantum entanglement," Rev. Mod. Phys. **81**, 865 (2009).

[44] J. Clarke and F. K. Wilhelm, Superconducting quantum bits, Nature (London) **453**, 1031 (2008).

[45] X. Gu, A. F. Kockum, A. Miranowicz, Y.-X. Liu, and F. Nori, Microwave photonics with superconducting quantum circuits, Phys. Rep. **718-719**, 1 (2017).

[46] J. Joo, W. J. Munro, and T. P. Spiller, Quantum metrology with entangled coherent states, Phys. Rev. Lett. **107**, 083601 (2011).

[47] M. Mirrahimi, Z. Leghtas, V. V. Albert, S. Touzard, R. J. Schoelkopf, L. Jiang, and M. H. Devoret, Dynamically protected cat-qubits: A new paradigm for universal quantum computation, New J. Phys. **16**, 045014 (2014).

[48] A. Almheiri, D. Marolf, J. Polchinski, and J. Sully, Black holes: Complementarity or firewalls? J. High Energy Phys. 02 (2013) 062.

[49] P. Hayden and J. Preskill, Black holes as mirrors: Quantum information in random subsystems, J. High Energy Phys. (2007) 120.

[50] S. D. Mathur, The information paradox: A pedagogical introduction, Class. Quantum Grav. **26**, 224001 (2009).

[51] K. A. Landsman, C. Figgatt, T. Schuster, N. M. Linke, B. Yoshida, N. Y. Yao, and C. Monroe, Verified quantum information scrambling, Nature (London) **567**, 61 (2019).